Bioactive Materials 41 (2024) 193–206

Contents lists available at ScienceDirect

Bioactive Materials

journal homepage: www.keaipublishing.com/en/journals/bioactive-materials

Injectable immunoregulatory hydrogels sequentially drive phenotypic polarization of macrophages for infected wound healing

Yuxiang Wang [a,b], Chen Zhou [a,b], Zhulian Li [a,b], Gong Li [a,b], Yaping Zou [a,b], Xing Li [a,b], Peiyang Gu [a,b], Jingyi Liu [a,b], Lang Bai [c], Hong Yan [d], Jie Liang [a,b,e], Xingdong Zhang [a,b], Yujiang Fan [a,b,**], Yong Sun [a,b,*]

[a] National Engineering Research Center for Biomaterials, Sichuan University, 29# Wangjiang Road, Chengdu, Sichuan, 610064, China
[b] College of Biomedical Engineering, Sichuan University, 29# Wangjiang Road, Chengdu, Sichuan, 610064, China
[c] Center of Infectious Diseases, West China Hospital of Sichuan University, 37# Guoxue Lane, Chengdu, Sichuan, 610041, China
[d] Department of Plastic, Aesthetic, Reparative and Reconstructive Surgery/Wound Repair Center, West China Second University Hospital of Sichuan University, 20# Section 3, South Renmin Road, Chengdu, Sichuan, 610041, China
[e] Sichuan Testing Center for Biomaterials and Medical Devices, Sichuan University, 29# Wangjiang Road, Chengdu 610064, China

ARTICLE INFO

Keywords:
Sequential immunoregulation
Macrophage phenotypic polarization
Injectable hydrogel
Infected wounds

ABSTRACT

Regulating macrophage phenotypes to reconcile the conflict between bacterial suppression and tissue regeneration is ideal for treating infectious skin wounds. Here, an injectable immunoregulatory hydrogel (SrmE20) that sequentially drives macrophage phenotypic polarization (M0 to M1, then to M2) was constructed by integrating anti-inflammatory components and proinflammatory solvents. *In vitro* experiments demonstrated that the proinflammatory solvent ethanol stabilized the hydrogel structure, maintained the phenolic hydroxyl group activity, and achieved macrophages' proinflammatory transition (M0 to M1) to enhance antibacterial effects. With ethanol depletion, the hydrogel's cations and phenolic hydroxyl groups synergistically regulated macrophages' anti-inflammatory transition (M1 to M2) to initiate regeneration. In the anti-contraction full-thickness wound model with infection, this hydrogel effectively eliminated bacteria and even achieved anti-inflammatory M2 macrophage accumulation at three days post-surgery, accelerated angiogenesis and collagen deposition. By sequentially driving macrophage phenotypic polarization, this injectable immunoregulatory hydrogel will bring new guidance for the care and treatment of infected wounds.

1. Introduction

The bacterial colonization of skin wounds usually stimulates the body to produce an inflammatory immune response and eliminate bacteria via the innate or adaptive immune system [1,2]. However, the autoimmune system cannot effectively clear the large amounts of invading bacteria in time after extensive skin damage. Escaping bacteria quickly form protective biofilms to enhance their adhesion on the skin surface and resist the infiltration of antibiotics and the killing effect of the body's immune substances [3,4]. At the same time, bacterial secretions can alter the wound microenvironment, causing chronic inflammation, seriously affecting skin healing, and even resulting in serious consequences such as bacteremia and ecthyma gangrenosum [5,6]. Although chemical drugs, antibiotics, and other methods have achieved good therapeutic effects in bacterial skin infections, increasing evidence has shown that drug abuse can lead to the emergence of drug-resistant bacteria [7–10]. Developing immunomodulatory biomaterials to address bacterial skin infections may be an effective treatment strategy in the face of the contradictory physiological processes of bacterial inhibition and tissue regeneration.

Macrophages are one of the representative cells in the process of immune regulation [11–14]. In recent years, studies on regulating macrophages' phenotypic polarization to treat bacterial infections and improve the healing of infected wounds have become a hot topic in the biomedical field. Proinflammatory (M1) macrophages can secrete various killer cytokines such as Interleukin (IL)-1β and tumor necrosis

Peer review under responsibility of KeAi Communications Co., Ltd.
* Corresponding author. National Engineering Research Center for Biomaterials, Sichuan University, 29# Wangjiang Road, Chengdu, Sichuan, 610064, China.
** Corresponding author. National Engineering Research Center for Biomaterials, Sichuan University, 29# Wangjiang Road, Chengdu, Sichuan, 610064, China.
E-mail addresses: fan_yujiang@scu.edu.cn (Y. Fan), sunyong8702@scu.edu.cn (Y. Sun).

https://doi.org/10.1016/j.bioactmat.2024.07.015
Received 30 April 2024; Received in revised form 26 June 2024; Accepted 12 July 2024
Available online 20 July 2024

factor (TNF)-α, or perform phagocytosis to help the body clear harmful substances [15–17]. In contrast, anti-inflammatory (M2) macrophages can secrete IL-10 and transforming growth factor (TGF)-β1 to inhibit the tissue inflammatory response and promote regeneration [18–20]. For example, a photo-crosslinked silk fibroin (SF) hydrogel containing borosilicate (BS) activated macrophages' inflammatory response, increased the expression of anti-inflammatory factors to promote their M2 transformation via the rapid release of BS, and achieved good wound results in streptozotocin-induced diabetes rats [21]. Lysosomal-targeted nanoparticles were endocytosed into macrophages to achieve photo-driven M1 polarization, effectively eliminating residual bacteria in tissues [22]. Porous magnesium alloy implants induced macrophage polarization towards the M1 phenotype through the early release of high concentrations of magnesium ions, enhancing their phagocytic function and potentially eliminating implant-related infections [23]. A gelatin-based hydrogel loaded with ultra-small manganese oxide nanoparticles eliminated bacteria by generating reactive oxygen species (ROS) and inducing macrophages' M1 polarization, then stimulated M2 macrophages as ROS dropped to a benign level to promote wound healing [24]. Therefore, the simple and effective sequential regulation of macrophage phenotypes, involving the early induction of macrophage M1 polarization to eliminate bacteria and the later sustained induction of M2 polarization to accelerate wound healing, may be an ideal means of dealing with infected skin wounds.

Polyphenol compounds and chitosan (CS) are natural antibacterial compounds with immunoregulatory properties that have been widely used in biomedical research [25–27]. Studies have shown that both polyphenols and CS can effectively inhibit inflammatory responses through their large numbers of phenolic hydroxyl and free amino groups, promoting macrophage polarization towards the regenerative M2 phenotype, making them ideal candidate material components for skin regeneration [28–30]. In addition, the high polarity of ethanol (EtOH) ensures full mutual dissolution with body fluids, and its high volatility guarantees efficient removal, making it the simplest and most efficient skin surface antibacterial agent. Inspired by the fact that EtOH may cause liver damage by inducing the activation of macrophages in the liver and exacerbating inflammatory reactions [31–33], we believe EtOH might also induce macrophages' M1 proinflammatory transformation at skin wounds for bacterial clearance. Therefore, the integration of polyphenols, CS, and EtOH is expected to achieve the sequential regulation of macrophage phenotypes (M0 to M1, then to M2) at infected wounds and reconstruct a suitable immune microenvironment to achieve stepwise bacterial clearance (M0 to M1) and skin regeneration (M1 to M2).

In this study, gallic acid (GA)-modified CS (CS-G) and dopamine (DOPA)- modified SF (SF-D) were successfully prepared for the later regulation of M2 macrophages and a regenerative protein microenvironment [34]. An EtOH and sodium periodate ($NaIO_4$) solution was introduced as an early M1 macrophage inducer and gel crosslinker to construct an injectable immunoregulatory hydrogel (SrmE20), which was expected to treat bacterial infected wounds by sequentially driving macrophage phenotypic polarization (Scheme 1). *In vitro* experiments confirmed that SrmE20 could induce the M1 polarization of macrophages in the early stage and effectively clear bacteria. As the EtOH was consumed, phenolic hydroxyl groups and cations in the SrmE20 network gradually induced the M2 polarization of macrophages, restoring the regenerative microenvironment. In the anti-contraction full-thickness wound model (Φ = 6 mm) infected with *Staphylococcus aureus* (*S. aureus*), SrmE20 quickly eliminated bacteria at the wound site and restored the anti-inflammatory microenvironment of M2 macrophages, accelerated neovascularization and collagen matrix deposition, and positively regulated the regeneration process of infected wounds. The SrmE20 injectable immunoregulatory hydrogel, which drives the phenotypic polarization of macrophages in a time-sequential manner,

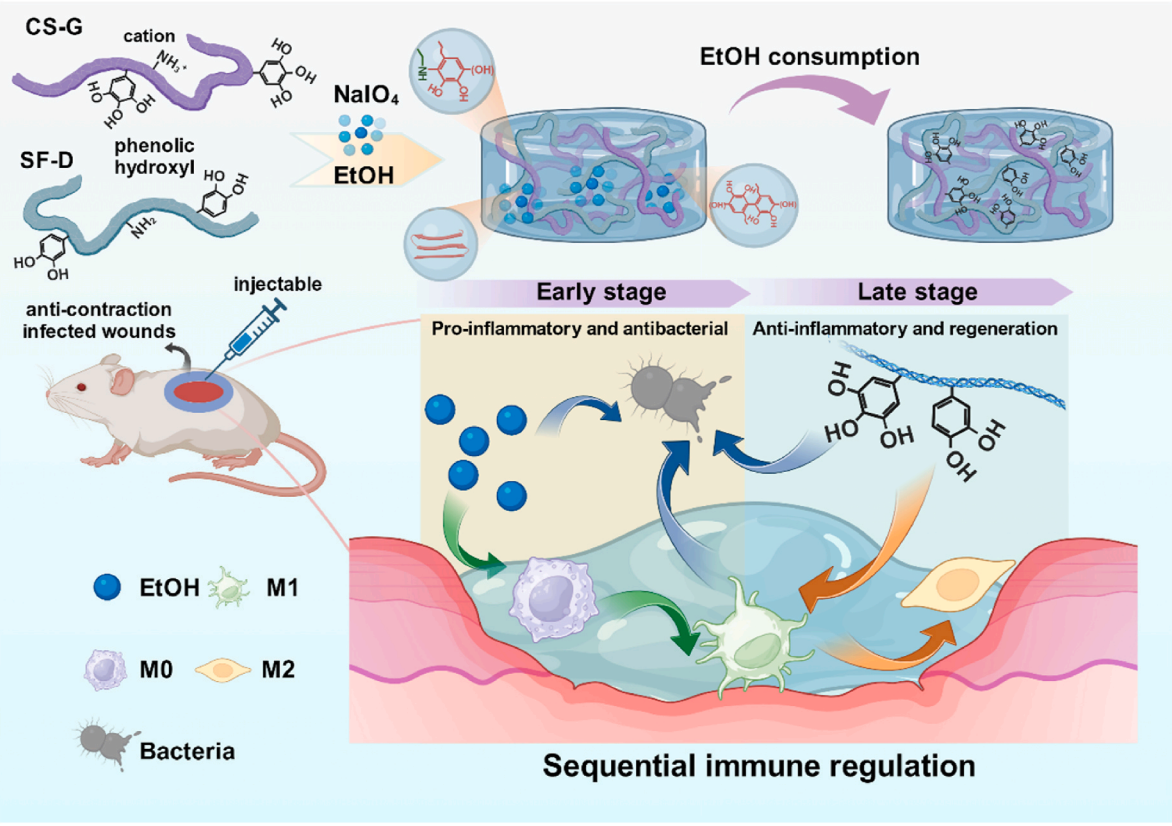

Scheme 1. Schematic illustration of injectable immunoregulatory hydrogel promoting infected wounds healing by sequentially driving macrophage phenotypic polarization.

will bring new biomaterial design inspiration for the treatment of bacterial infected wounds.

2. Materials and methods

2.1. Materials

Bombyx mori L. cocoons were purchased from Chengdu Chuansi Cocoon Co., Ltd., China. Chitosan (Mw = 100 kDa) and pronase E were obtained from Shanghai yuanye Bio-Technology Co., Ltd., China. Gallic acid monohydrate (GA·H_2O), $NaIO_4$, and EtOH was purchased from Chengdu Chron Chemicals, Co., Ltd., China. Dopamine hydrochloride (Dopa·HCl, 99 %), 1-Ethyl-3-(3-dimethyllaminopropyl) carbodiimide hydrochloride (EDC, 99 %), and N-hydroxysuccinimide (NHS, 99 %) were provided by Chengdu Best Reagent Co., Ltd., China. Lysozyme, tryptone soy broth, and tryptic soy agar were bought from Beijing Solarbio Science & Technology Co.,Ltd., China. DMEM medium (Hyclone), α-MEM Medium (Hyclone), and Penicillin-Streptomycin were bought from Thermo Fisher Scientific Inc., USA. Fetal bovine serum (FBS, Gibco, Australia origin) was obtained from Life Technologies Corporation, USA.

2.2. Preparation and characterization of CS-G and SF-D

645 mg chitosan was completely dissolved in a 2 % hydrochloric acid solution, then 760 mg GA H_2O, 850 mg EDC and 510 mg NHS were added at a pH of 4.75–5 under the protection of nitrogen. After 24 h, the reaction solution was collected and dialyzed against 1 ‰ hydrochloric acid solution for 3 days. CS-G was obtained by freeze-drying the dialysate. Silk fibroin was extracted from *Bombyx mori* L. cocoons using previously reported methods [35]. 1 g SF was configured to 150 mL reverse osmosis (RO) water at room temperature, and 959 mg EDC and 230 mg NHS were added to activate carboxyl for 1.5 h at a pH of 4.75–5. After that, 190 mg Dopa·HCl was added and the reaction was protected by nitrogen for 24 h. Then the reaction solution was collected and dialyzed against RO water for 3 days. SF-D was obtained by concentrating the dialysate. CS-G and SF-D were tested by Fourier transform infrared spectroscopy (FTIR; ATR, Invenio R, Germany) and ^1H nuclear magnetic resonance (^1H NMR; 400 MHz, Bruker AV II-400MHz, Switzerland), and detected with Folin & Ciocalteu's phenol reagent (Sigma-Aldrich, USA) to calculate polyphenol content.

2.3. Preparation and optimization of hydrogels

Different concentrations of $NaIO_4$ solution (1 mg/mL, 0.7 mg/mL, 0.5 mg/mL, 0.3 mg/mL, 0.1 mg/mL) and different ethanol ratios (5 %, 10 %, 15 %, 20 %) of 0.3 mg/mL $NaIO_4$ solution were prepared as crosslinking agents. 35 mg/mL SF-D and CS-G were mixed in equal proportions, and hydrogels were prepared by adding different crosslinking agents according to the volume ratio of 4:1. Finally, three hydrogels containing 0.3 mg/mL of $NaIO_4$ and 0 %, 5 %, and 20 % EtOH were obtained, which were named as SrmE0, SrmE5, and SrmE20, respectively. The gelation time of hydrogels was measured by the tube inversion. The SrmE5-R and SrmE20-R were obtained by removing EtOH after soaking SrmE5 and SrmE20 in sufficient PBS for 24 h, respectively.

2.4. Physicochemical properties characterization

The antioxidant capacity of hydrogels was obtained by incubating 100 mg hydrogels with 1 mL 0.2 mM DPPH ethanol solution at 37 °C for 1 h, and measuring the solution's absorbances at 517 nm. The mechanical properties analysis was performed by dynamic mechanical test (TA-Q800, USA) under the multi-frequency mode (a fixed frequency of 1–10 Hz, an amplitude of 40 μm, a preload force of 0.002 N, and a force track of 105 %) at constant room temperature. The conformational changes of proteins were measured by FTIR. The pore structures of hydrogels were observed by Scanning electron microscopy (SEM; HITACHI S-800, Japan) after coated with gold. The swelling properties of hydrogels were obtained by soaking in phosphate-buffered saline (PBS) solution at 37 °C for a specific time and weighing wet weight. The degradation behavior was obtained at 37 °C by soaking hydrogels in 5 U/mL pronase E solution and 3 mg/mL lysozyme for different times, respectively. The protein adsorption capacity of hydrogels was measured through the Pierce BCA Protein Assay Kit (Thermo Fisher).

2.5. Cell proliferation and migration

100 μL cylindrical hydrogel (Φ = 8 mm) and 5000 NIH-3T3 cells were cultured together in 1 mL DMEM complete medium in an incubator at 37 °C under 5 % CO_2 conditions. The medium was changed every two days. At a specific time, cells were harvested and measured by cell counting kit-8 (Dojindo, Japan). Cell proliferation was evaluated by measuring OD value after the active ingredients in CCK-8 reduced by dehydrogenase in mitochondria to produce highly water-soluble orange yellow formazan products. 3×10^5 NIH-3T3 cells were planted on the surface of the hydrogel, cultured for a specific time, and then stained with Fluorescein diacetate/propidium iodide (FDA/PI) for observing by laser scanning confocal microscopy (LSCM, LSM880, Germany). Transwell (8 μm, Corning, USA) model was used to investigate the ability of hydrogel to promote cell migration. Hydrogels (100 μL, Φ = 8 mm) were placed with 600 μL α-MEM medium containing serum below the well. Then, 100 μL bone marrow mesenchymal stromal cells (BMSCs) suspension (1.2×10^5 cells/mL, serum-free) from rabbits was added to Transwell and incubated in an environment of 37 °C and 5 % CO_2 for 24 h. The Transwell was collected and fixed with paraformaldehyde (4 %). After staining with crystal violet and removing impurities, cell migration was observed under a microscope. Afterwards, the crystal violet on Transwell was dissolved in 33 % acetic acid ethanol solution and measured the absorbance at 562 nm.

2.6. Antibacterial activity in vitro

The antibacterial ability of hydrogels *in vitro* was evaluated by *Escherichia coli* (*E. coli*) and *S. aureus*. 10^5 CFU *E. coli* and *S. aureus* were cultured in liquid medium with 200 μL hydrogel overspreading the bottom of plate for 12 h, respectively. Then, the bacterial liquid were diluted 10^6 times for spread plate method, and the bacterial colony was observed after 20 h 10^5 CFU *E. coli* and *S. aureus* were cultured in liquid medium with 150 μL cylindrical hydrogel (Φ = 8 mm) for 12 h, respectively. Then the hydrogel was collected and fixed with paraformaldehyde to observe the morphology of bacteria by SEM. In addition, 100 μL cylindrical hydrogel was incubated with 10^7 CFU *E. coli* and *S. aureus* for 24 h, respectively. These hydrogels were collected and washed by PBS for many times. Fluorescent staining was performed according to the instructions of Baclight kit (Thermo Fisher) to observe the bacteria on the surface of hydrogels by LSCM.

2.7. Macrophages polarization induced by hydrogels

5×10^5 RAW 264.7 cells and 300 μL hydrogel were cultured together under standard conditions, and the medium was changed every two days. Cells and supernatants were collecting after 2 and 4 days, respectively. After marking with FITC anti-mouse CD86 antibody and APC anti-mouse CD206 antibody (biolegend, USA), the phenotype of macrophages was identified by flow cytometry (LSRFortessaTM X-20, USA). The control group without the SrmE20 gel was cultured for two and four days, and named M0-2D and M0-4D, respectively. The concentration of cytokines in supernatants were detected using Elisa assay kit (Dakewe, China), including IL-1β, IL-10, TNF-α, and TGF-β. Immunofluorescence (IF) staining for CD86/CD206 (19589/24595, Cell signaling technology, USA) was implemented. In addition, 100 μL

cylindrical hydrogel was implanted into the leg muscles of SD rats, and the hydrogel and surrounding tissues were collected after one day and four days for IF staining to evaluate the effect of the hydrogel on driving the phenotype polarization of macrophages sequentially *in vivo*.

2.8. In vivo wound healing evaluation by infected full-thickness skin defect model

The animal experiments were approved by the Sichuan University Medical Ethics Committee (KS2020330) and all the animal procedures were performed in accordance with the Guidelines for the Care and Use of Laboratory Animal of Sichuan University. 6 weeks male KM mice (Chengdu Dossy, China) were raised one week in advance to adapt to the environment. After anesthetized and skin preparation, round full-thickness wounds with a diameter of 6 mm were made on both sides of their spine. Then, clamp plates were secured around the wounds to prevent wound contraction. 100 μL *S. aureus* (10^7 CFU/mL) was dripped onto wounds surface for infection. One day after bacterial infection, 100 μL hydrogel was used for wound repair. Tegaderm and elastic bandage (3 M, USA) were used for wound protection throughout the treatment. Gross observation was performed after mice sacrificed at a specific time, and bacteria on wounds surface were collected for spread plate method. The new skin tissue was fixed with paraformaldehyde and examined histologically.

2.9. Histological analysis

The skin tissue was cut into 6 μm paraffin sections for histological staining. The wound recovery was observed by HE, the bacteria inside the tissue were observed by Gram positive staining, and collagen production in the new skin was examined by Masson staining and Sirius Red staining. The polarization of macrophages at the wound was observed by CD86/CD206 IF staining. Blood vessels were verified by Platelet endothelial cell adhesion molecule 1 (CD31; ab182981, Abcam, UK) IF staining, and hair follicles were confirmed by keratin 5 (Krt 5; GB111246, Servicebio, China) IF staining.

2.10. Statistical analysis

Each experiment was independently repeated at least 3 times with similar results. All data were presented as mean ± standard deviation (SD) of at least three representative experiments. GraphPad Prism 8 software was used for statistical analysis using one-way ANOVA and student's *t*-test. The difference was statistically significant at three levels. *P < 0.05, **P < 0.01, and ***P < 0.001.

3. Results

3.1. Optimization and characterization of injectable immunoregulatory hydrogels that sequentially regulate of macrophage phenotypes (Srm hydrogels)

To prepare injectable immunoregulatory hydrogels that sequentially drive phenotypic polarization of macrophages, GA and DOPA were first grafted onto the molecular chains of CS and SF via an amide reaction (Figs. S1A and B), respectively. The ^{1}H NMR peaks at 7–7.5 and 8–8.5 ppm confirmed the presence of the pyrogallol and catechol groups (Figs. S1C and D). The ultraviolet absorption spectrum showed the success of the grafting reaction (270 nm; Figs. S1E and F). FTIR showed the integrity of the CS and SF molecular chains (Figs. S1G and H). The grafting rates of CS-G and SF-D were 6.602 % and 4.985 %, respectively.

The addition ratios of $NaIO_4$ and EtOH were optimized through gelation performance and mechanical characteristics (Fig. 1A). A high $NaIO_4$ concentration caused the oxidation reaction to occur rapidly, and the pre-crosslinking solution completed crosslinking within a few seconds. As the $NaIO_4$ concentration decreased, the gelation time increased, and it could not be crosslinked within 30 min at 0.1 mg/mL (Figs. S2A and B). The 2,2-diphenyl-1-picrylhydrazyl (DPPH) scavenging rate was related to the residual phenolic hydroxyl groups in the hydrogel, which were opposite to the degree of oxidation. Fig. S2C showed that hydrogels at 0.3 mg/mL $NaIO_4$ had the highest DPPH scavenging rate, indicating the lowest degree of oxidation and the most residual phenolic hydroxyl groups. The hydrogels' mechanical strength gradually increased as the $NaIO_4$ concentration decreased, and the storage modulus was the highest at 0.3 mg/mL (Figs. S2D and E), potentially because the tiny bubbles in the hydrogel were effectively excluded in the slow crosslinking. Therefore, 0.3 mg/mL $NaIO_4$ was preferred.

At the determined $NaIO_4$ concentration, adding EtOH affected the gelation performance. As the EtOH concentration increased, the gelation time first decreased, then increased, and then decreased (Figs. S3A and B). Compared to the hydrogel without EtOH (SrmE0), the hydrogels containing EtOH had lower degree of oxidation and more active phenolic hydroxyl groups, which was reflected by their increased relative DPPH scavenging rate, with 20 % EtOH performing best (Fig. 1B). All EtOH concentrations enhanced the mechanical properties of the hydrogels (Fig. 1C and S3C). Based on FTIR, adding EtOH introduced an additional gelation method, β-sheet, and the proportion of β-sheet in the protein increased with the EtOH content (Fig. 1D). The opposing trends of oxidation degree and β-sheet content in the hydrogels indicated an antagonistic relationship between the two gelation methods based on EtOH and $NaIO_4$ (Fig. 1E). NIH-3T3 fibroblasts cytotoxicity assay confirmed that even at the set maximum EtOH concentration (20 %) cells had ≥75 % viability (Fig. S3D).

Through optimization, three hydrogels (SrmE0, SrmE5, and SrmE20) containing 0.3 mg/mL of $NaIO_4$ and 0 %, 5 %, or 20 % EtOH were selected for physicochemical characterization. These hydrogels showed good injectability and could adhere to the skin surface with complex morphology, such as finger joints (Fig. 1F and G; Supporting Video 1). The hydrogels could also adapt to the complex physiological environment and skin deformation and stably adhere to the pig skin even when it was subjected to large twisting or liquid immersion (Fig. 1H; Supporting Video 2). SEM observed that the three hydrogels all had connected porous structures, and adding EtOH significantly increased the pore size. However, SrmE5 and SrmE20 did not differ significantly (Fig. 1I and J). The swelling capacity of the hydrogels increased with the EtOH concentration, and SrmE20 reached the maximum swelling rate of more than twentyfold in 30 min (Fig. 1K). The hydrogels could be biodegraded by various enzymes, and SrmE20 had the fastest degradation rate (Fig. 1L and M). Adding EtOH also increased the protein adsorption capacity of the hydrogels, and SrmE20 showed significantly higher protein adsorption than SrmE0 and SrmE5 (Fig. 1N).

Supplementary video related to this article can be found at https://doi.org/10.1016/j.bioactmat.2024.07.015

3.2. Effects of Srm hydrogels on cell proliferation and migration

Fig. 2A showed the cell compatibility test of the hydrogels in CCK-8 and Live/Dead staining. Due to the addition of EtOH, cell activities were lower in the SrmE5 and SrmE20 groups than in the SrmE0 group at one day. However, cell proliferation gradually increased after EtOH was removed with the change of culture medium at 3, 5, and 7 days (Fig. S4). On the third day, cell activity was significantly higher in the SrmE5 and SrmE20 groups than in the SrmE0 group, with the SrmE20 group showing the greatest ability to promote cell proliferation in the later stage (Fig. 2B). The FDA/PI staining presented that the addition of EtOH weakened the growth of cells on the hydrogels' surface at one day. However, after EtOH removal by medium replacement, the SrmE5 and SrmE20 groups had better cell proliferation after 3 days. (Fig. 2C).

Fig. 2D showed the experimental process of the hydrogel regulating BMSCs migration. The SrmE5-R and SrmE20-R were obtained by removing EtOH by soaking SrmE5 and SrmE20 in sufficient PBS for 24 h, respectively. The results showed that compared to the SrmE0 group, the

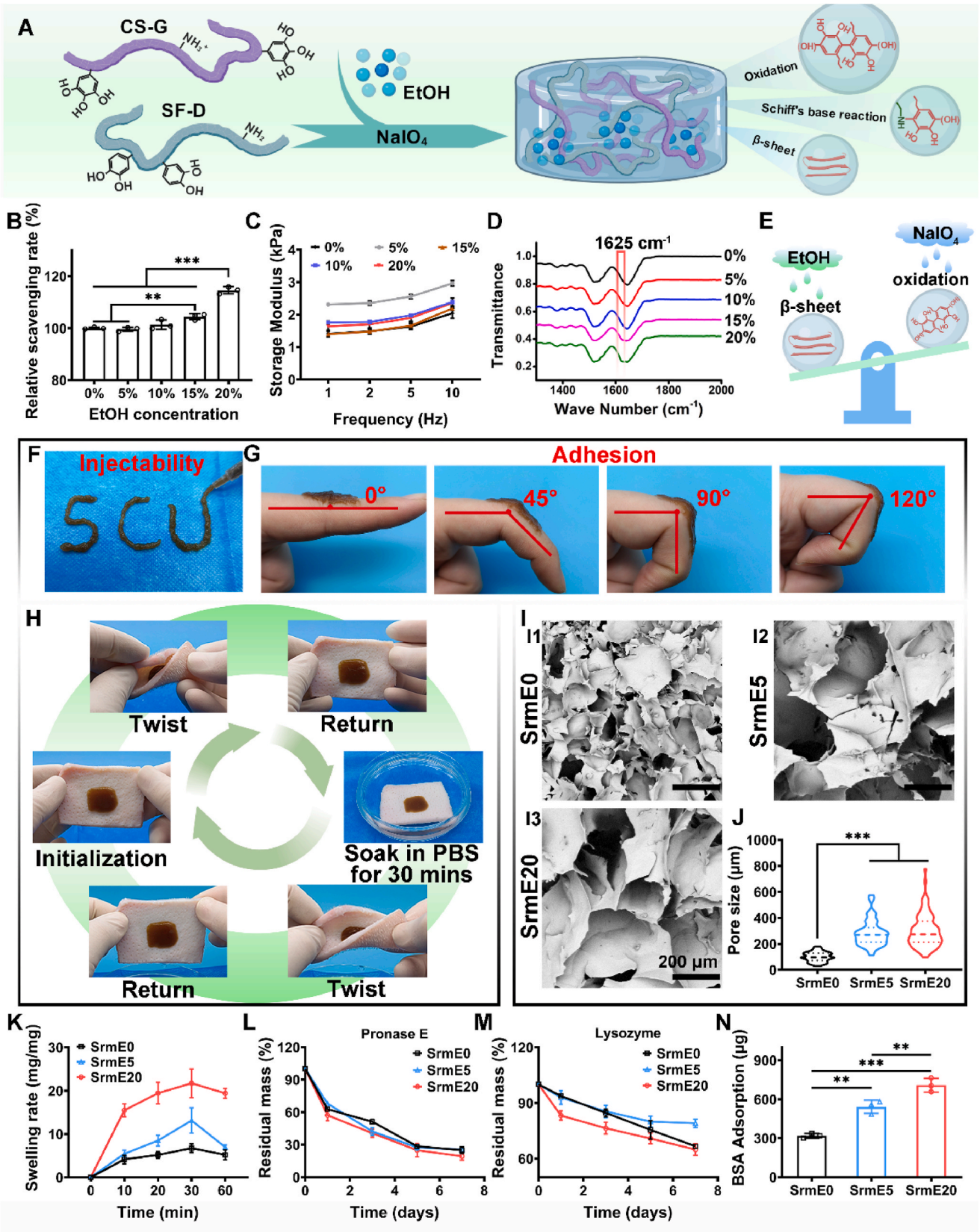

Fig. 1. (A) Schematic diagram of the preparation of injectable Srm hydrogels. (B) Relative free radical scavenging rate, (C) storage modulus, and (D) FTIR spectra of hydrogels at different EtOH concentrations. (E) The antagonistic relationship between two gelation methods. (F) Injectability, (G) adhesion, and (H) adaptation to skin twisting and liquid physiological environment of the hydrogel. (I) Microstructure of the hydrogels using SEM analysis. (J) Inner pore diameter analysis of specimens. (K) Swelling behavior of the hydrogels. Degradation behavior under the action of (L) pronase E and (M) lysozyme. (N) Protein adsorption capacity test. *p < 0.05, **p < 0.01, and ***p < 0.001.

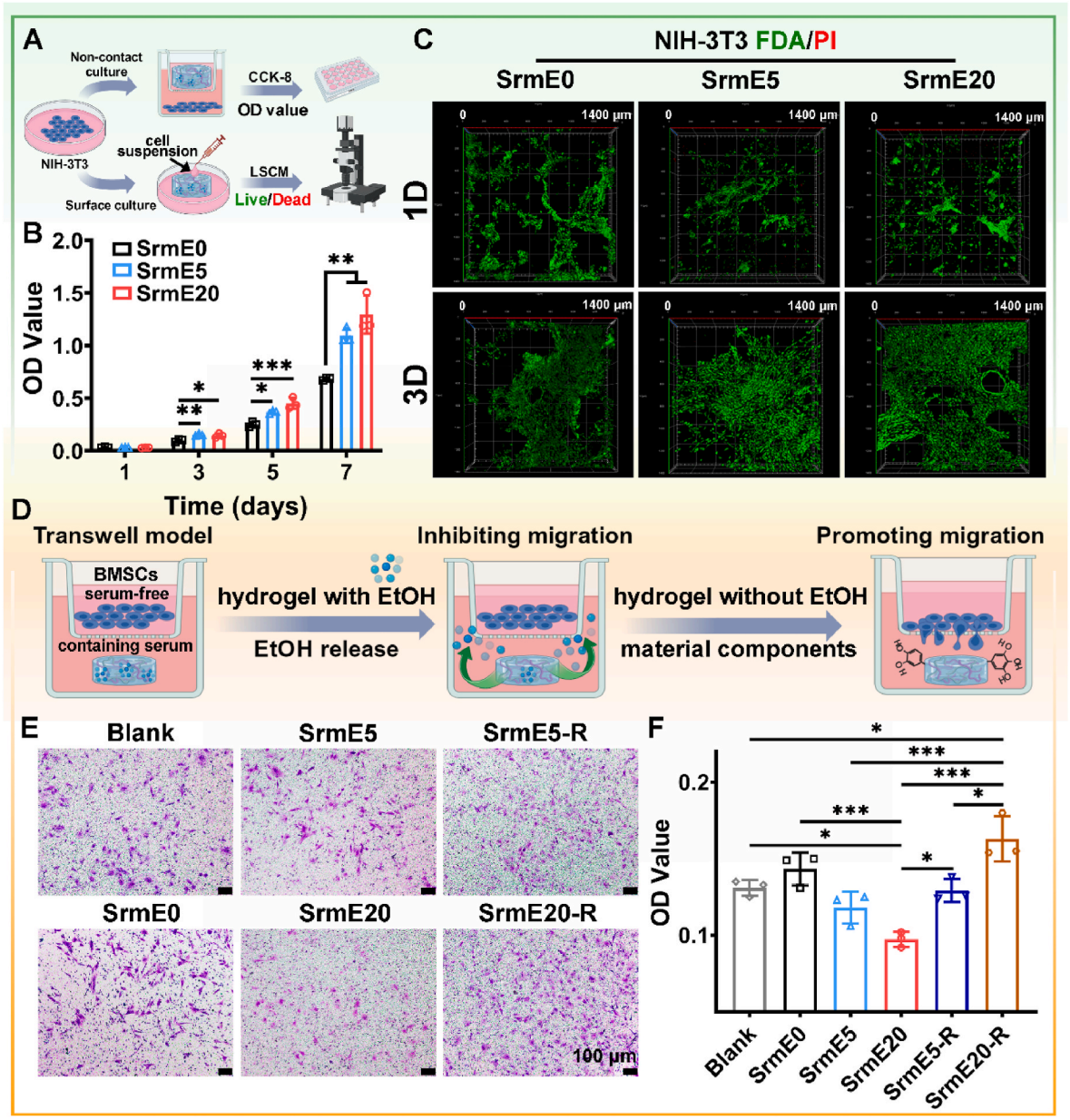

Fig. 2. (A) Schematic diagram of NIH-3T3 cell proliferation in CCK-8 and FDA/PI staining. (B) Cell viability of NIH-3T3 cultured after different times in non-contact culture. (C) Live/dead staining in surface culture. (D) Schematic diagram of BMSCs migration in a Transwell model. (E) Crystal violet staining of migrated cells. (F) Migration cells statistics. *p < 0.05, **p < 0.01, and ***p < 0.001.

SrmE5 and SrmE20 groups could inhibit cell migration, of which SrmE20 had the weakest ability to promote cell migration in the early stage. However, SrmE5-R and SrmE20-R could reverse the inhibitory effect of EtOH and significantly promote cell migration after EtOH removal, of which SrmE20-R had the best ability to promote cell migration (Fig. 2E and F). These results suggested that hydrogels containing EtOH could inhibit cell proliferation and migration at the early stage via EtOH and promote cell proliferation and migration after EtOH removal, indicating the ability to regulate cell behavior in a time-sequential manner.

3.3. *In vitro* antibacterial ability of Srm hydrogels

Based on material design, the Srm hydrogels have potential antibacterial activity via three mechanisms. First, as a common surface antibacterial agent, EtOH has a natural inhibitory function on bacteria. Second, the large number of free amino groups in CS are believed to interact with the negatively charged outer membrane of bacteria, disrupting their structure. Third, the antibacterial effects of polyphenols have been widely reported (Fig. 3A). The hydrogels' inhibitory effects on *E. coli* and *S. aureus* were confirmed by various methods (Fig. 3B and S5). Fig. 3C showed the results of the spread plate method after co-culturing bacteria with the hydrogels. The number of bacteria in SrmE0 group was less than that in the control group, which confirmed the antibacterial property of the material itself. Furthermore, the number of bacteria in SrmE5 and SrmE20 groups gradually reduced, proving that the increased EtOH improved antibacterial effect, with SrmE20 having the best antibacterial effect (Fig. 3C–E). After washing away dead and stray bacteria, fluorescence staining of the living bacteria showed that the fluorescence intensity was significantly lower on SrmE20 (Fig. 3F). The semi-quantitative results of integral optical density (IOD) also proved that adding EtOH effectively reduced the adhesion of bacteria to the hydrogel, which was more apparent for *S. aureus* (Fig. 3F–H). Similarly, the morphology of bacteria adhering on the

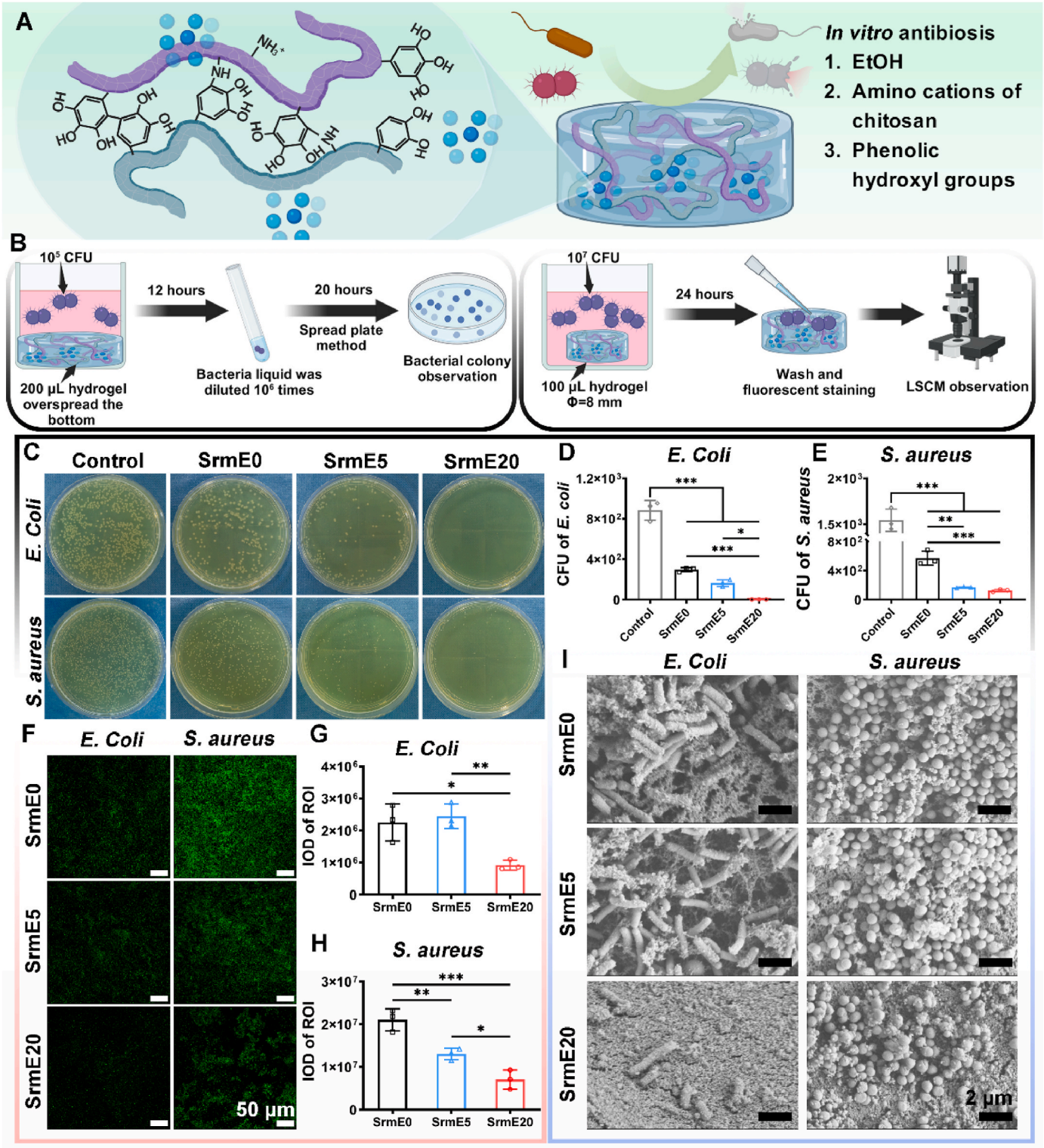

Fig. 3. (A) Potential antibacterial mechanisms of the Srm hydrogels. (B) Schematic diagram of antibacterial experiments *in vitro*. (C) The bacteria in the spread plate method. Colonies count statistics of (D) *E. coli* and (E) *S. aureus*. (F) Fluorescence staining of living bacteria and corresponding integral optical density (IOD) statistics on (G) *E. coli* and (H) *S. aureus*. (I) Bacterial morphology using SEM analysis. *p < 0.05, **p < 0.01, and ***p < 0.001.

hydrogel's surface was observed by SEM (Fig. 3I), which showed fewer bacteria on the SrmE20 with changed size and morphology, proving its effective bacterial inhibition.

3.4. SrmE20 sequentially drove phenotypic polarization of macrophage

The experiment illustrated in Fig. 4A was used to demonstrate the time-sequential driving of macrophage's phenotypic polarization by SrmE20 *in vitro*. Flow cytometry showed that on the second day, the $CD206^{+}/CD86^{+}$ macrophage ratio was 3.371 in the M0 group and 1.384

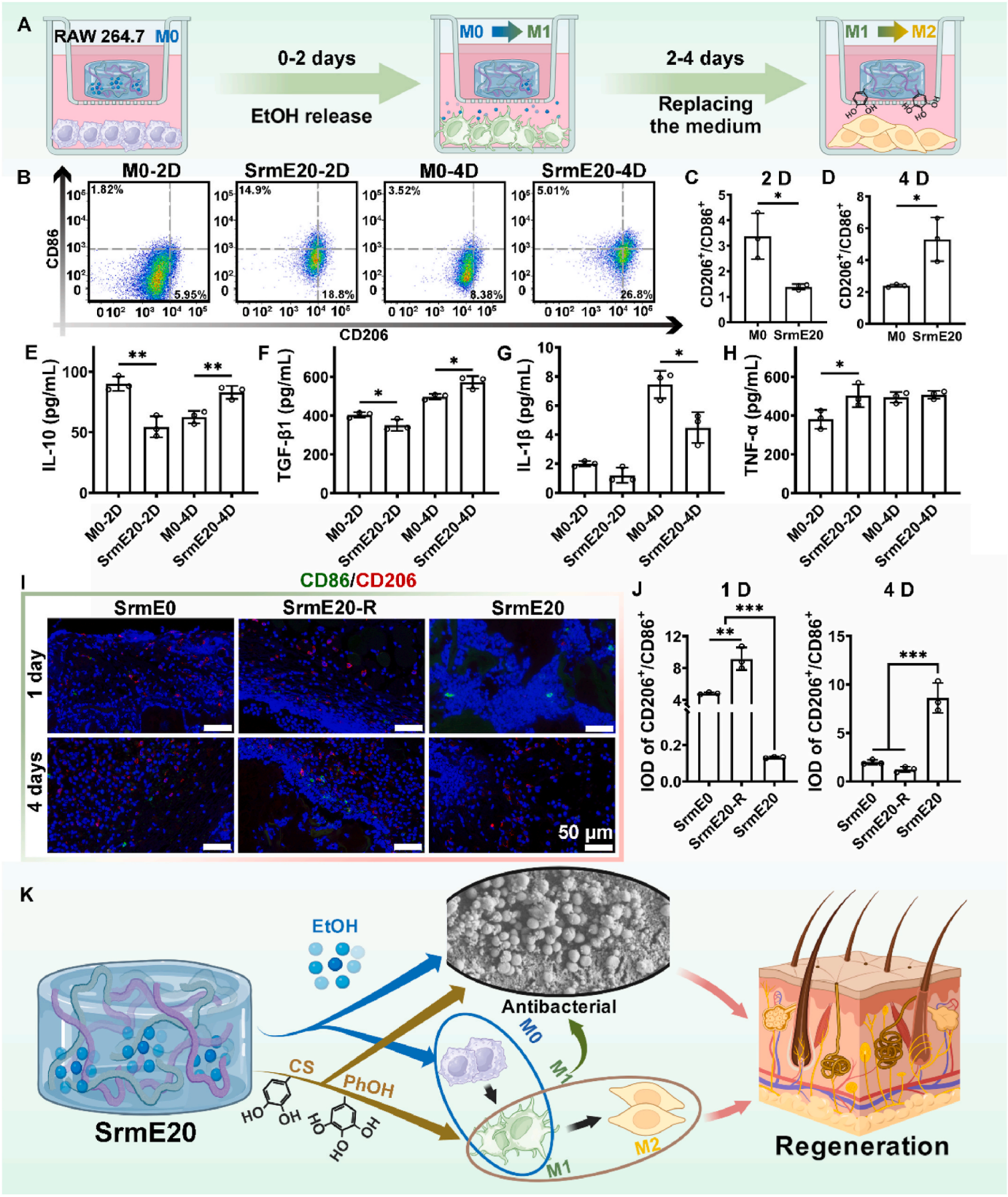

Fig. 4. (A) Schematic diagram of driving macrophage phenotypic polarization test *in vitro* using RAW 264.7. (B) Representative flow cytometry plots and statistics for $CD206^{+}/CD86^{+}$ macrophages at (C) 2 days and (D) 4 days. Expression of inflammatory factors including (E) IL-10, (F) TGF-β1, (G) IL-1β, and (H) TNF-α. (I) Representative CD86/CD206 IF staining of macrophages in intramuscular implantation experiments and (J) IOD statistics of fluorescence intensity. (K) Schematic illustration of the hydrogels used for infected wounds. *$p < 0.05$, **$p < 0.01$, and ***$p < 0.001$.

in the SrmE20 group, proving that SrmE20 significantly induced macrophages to M1 type in the early stage. On the fourth day, the $CD206^+$/$CD86^+$ macrophage ratio was 2.383 in the M0 group and 5.300 in the SrmE20 group, confirming significant M2 macrophage polarization in the SrmE20 group (Fig. 4B–D). The detection of cytokines also confirmed the sequential polarization of macrophages. On the second day, macrophages in the SrmE20 group secreted significantly more TNF-α (M1 macrophage marker) but significantly less IL-10 and TGF-β1 (M2 macrophage markers) than those in the M0 group, indicating that SrmE20 stimulated the M1 polarization of macrophages after two days. In contrast, on the fourth day, IL-10 and TGF-β1 secretion had significantly increased while IL-1β (M1 macrophage marker) had significantly decreased in the SrmE20 group, demonstrating that M1 macrophages had been successfully induced to the M2 phenotype (Fig. 4E–H). In IF staining for CD86 (green) and CD206 (red), the color of macrophages changed into green after two days and into red after four days in the SrmE20 group, indicating their significantly continuous polarization from M0 to M1 and then to M2 (Figs. S6A and B). In the intramuscular implantation experiment, SrmE20 drove more M1 macrophages to polarization at one day, manifested by more CD86 green fluorescence and lower $CD206^+/CD86^+$ values, while in contrast, more M2 macrophages were found in the two control groups without EtOH. On the fourth day, SrmE20 had more M2-type polarized macrophages than the other groups (Fig. 4I and J). These results confirmed that SrmE20 could effectively sequentially drive phenotype polarization of macrophages *in vivo*.

These results confirmed that SrmE20 could drive the polarization of macrophages from M0 to M1 in the early stage, exerting proinflammatory effects, and from M1 to M2 in the later stage, exerting anti-inflammatory effects, demonstrating its function of continuously and time-sequentially driving phenotypic polarization of macrophage (Fig. S6C). Based on this sequential immune regulation function, SrmE20 was expected to be useful for treating infected wounds. In the early stage, the antibacterial effect was accelerated through hydrogel components (EtOH, CS, polyphenols) and the induction of M1 macrophage polarization. In the later stage, the M2 polarization of macrophages was induced after the removal of bacteria to improve wound healing (Fig. 4K).

3.5. Bacterial clearance in anti-contraction infected wounds by Srm hydrogels

An anti-contraction full-thickness wound model infected with *S. aureus* (Φ = 6 mm) was used to investigate the ability of SrmE20 to promote the regeneration of infected wounds (Fig. 5A). Gross observations demonstrated that bacterial films and pus appeared one day after *S. aureus* inoculation, indicating severe wound infection. The SrmE20 group was characterized by minimal infection after three days, with the wounds basically closed after seven days and appearing like normal skin after 16 days (Fig. 5B and S7). The statistical wound area results showed that the SrmE20 group had the fastest closure rate and the smallest remaining area (Fig. 5C). The bacteria on the wound surface were examined using the spread plate method. The results showed that the bacteria in the Blank group continued to proliferate, and using the hydrogel effectively reduced the number of bacteria. The SrmE20 group had the best antibacterial effect, with a relative antibacterial rate of 88.52 % at three days and 97 % at seven days compared to the Blank group (Fig. 5D and E). Since bacteria would form biofilms within tissues to escape immune clearance, Gram-positive staining was used to track *S. aureus* within skin tissue (Fig. 6A, green arrow). It was apparent that many bacteria grew into newly formed tissues in the Blank group with a wide distribution. In contrast, the positive staining was decreased in the SrmE0 and SrmE20-R groups, although bacteria still penetrated deep into the tissue. However, only a small amount of bacterial staining was observed in the SrmE20 group at three days, and no bacteria were observed inside the skin at seven days. All these data indicated that SrmE20 could effectively inhibit bacteria in infected wounds and prevent bacterial colonization within tissues.

3.6. SrmE20 promoted skin healing through phenotypic polarization of macrophage

Due to the rapid clearance of bacteria, macrophages in the SrmE20 group had already started M2 polarization at three days, while the other groups still had severe inflammatory responses. At seven days, M2-type macrophages were further increased in the SrmE20 group, indicating a steady regenerative progression. In contrast, the other groups produced more M1-type macrophages for bacterial clearance and phagocytosis (Fig. 6B–F).

Fig. 6G and S8 showed the healing process of the infected wound. The SrmE20 group had the fastest re-epithelialization process, and the newly formed epidermis had an evidently curved morphology similar to the natural skin. In the newborn skin, earlier collagen deposition was observed in the SrmE20 group, which was 2–3 times higher than in the other groups at seven days. There was also little difference between collagen content at seven days and 16 days, indicating the maturation of the newborn skin in the SrmE20 group (Fig. 7A–C). In addition, the new skin showed interwoven collagen fibers with a wide distribution of arrangement angles similar to normal skin in the SrmE20 group. However, the range of collagen fiber arrangement angles was narrow in the other groups, suggesting the fate of scarring (Fig. 7D and E). CD31 labeling showed that vascularization occurred earliest in the SrmE20 group, with the positive expression of CD31 significantly higher in the other groups at seven days. As the skin matured, blood vessels gradually decreased with the positive CD31 expression (Fig. 7F–H). The regeneration of hair follicle tissue was confirmed by Krt 5 staining (Fig. 7I, red arrow), with apparent hair follicle structures appearing at the wound edge of the SrmE20 group, suggesting that this hydrogel had the potential to initiate hair follicle regeneration from the edge to the center.

4. Discussion

The threat of bacterial infection to the body comes not only from its direct harm but also from the residual lipopolysaccharides (LPS) and peptidoglycans after bacterial fragmentation, as well as the cell damage. M1 macrophages are the main scavengers [36,37]. Drugs or photodynamic/photothermal antibacterial agents have significant therapeutic effects on killing bacteria on the surface of wounds. However, removing residual bacterial debris still relies on the body's killing cells, which may prolong the inflammatory phase of skin repair and affect wound healing [38]. The immune regulatory function of M2 macrophages has been reported in skin wound repair. However, inopportune anti-inflammatory changes may affect the clearance of bacteria and residues from infected wounds, and excessive M2 macrophages are also considered a cause of tissue fibrosis [39–41]. Therefore, it may be ideal to shorten the inflammatory period of infected wounds and promote skin healing via the early activation of M1 macrophage polarization for antibacterial effects and the clearance of bacterial-related products before later inducing M2 polarization.

The special biochemical functions of polyphenolic materials are believed to originate from their abundant phenolic hydroxyl groups [27,29]. Research has shown that some polyphenols can promote intracellular levels of cyclic adenosine monophosphate through dopamine receptor D1 and inhibit the activation of NLR family pyrin domain containing 3 inflammasomes to exert anti-inflammatory effects [42]. In addition, dopamine receptor D2 could negatively regulate NF-κB pathway and reduce the expression of inflammatory factors [43]. D1 receptors signaling could inhibit the LPS activation of macrophages, the function of monocytes, and the production of inflammatory cytokines [44]. Therefore, polyphenols are commonly used as induction materials for M2 macrophages in skin repair. However, in the oxidative cross-linking process triggered by $NaIO_4$, many phenolic hydroxyl groups are

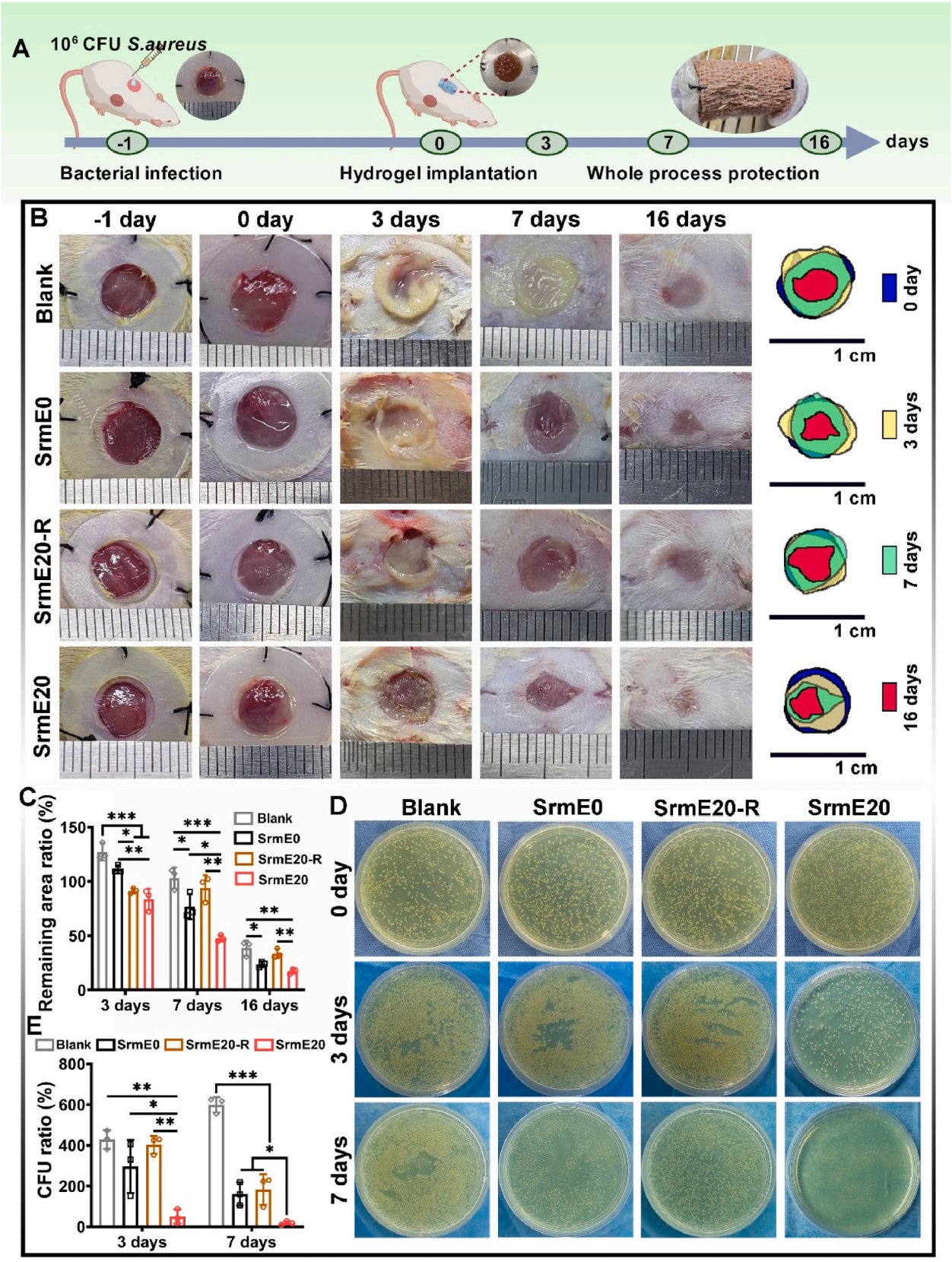

Fig. 5. (A) Schematic diagram for anti-contraction infected wounds healing. (B) Representative gross observation of infected wounds and superposition images. (C) Statistics of the remaining area of the wounds. (D) The spread plate method of bacteria on the surface of wounds and (E) colonies count statistics. *$p < 0.05$, **$p < 0.01$, and ***$p < 0.001$.

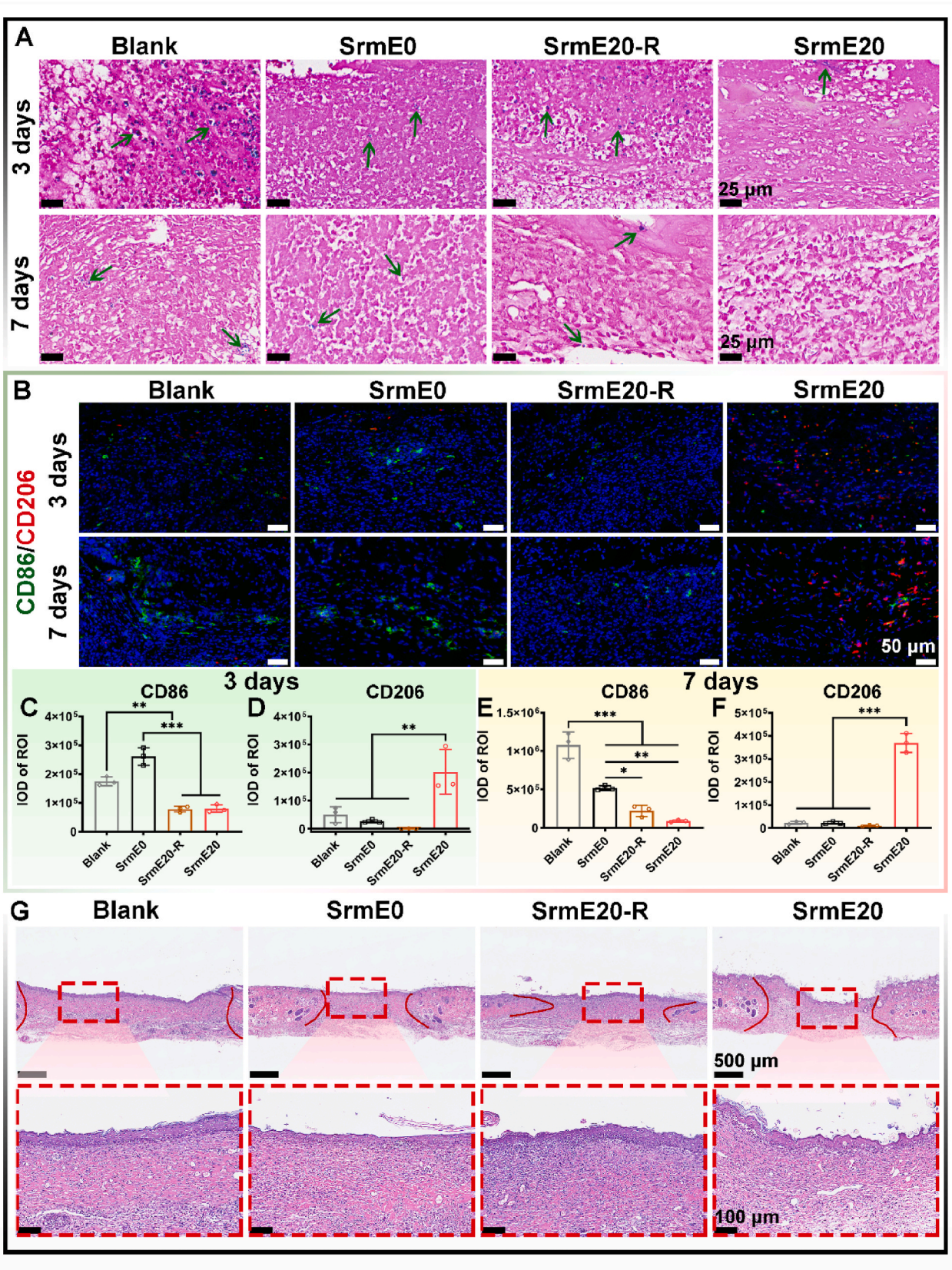

Fig. 6. (A) Gram-positive staining for bacterial within the wounds. (B) Representative CD206/CD86 immunostainings of macrophages. Fluorescence intensity statistics of (C) CD86 and (D) CD206 at three days. Fluorescence intensity statistics of (E) CD86 and (F) CD206 at seven days. (G) HE staining at 16 days. *$p < 0.05$, **$p < 0.01$, and ***$p < 0.001$.

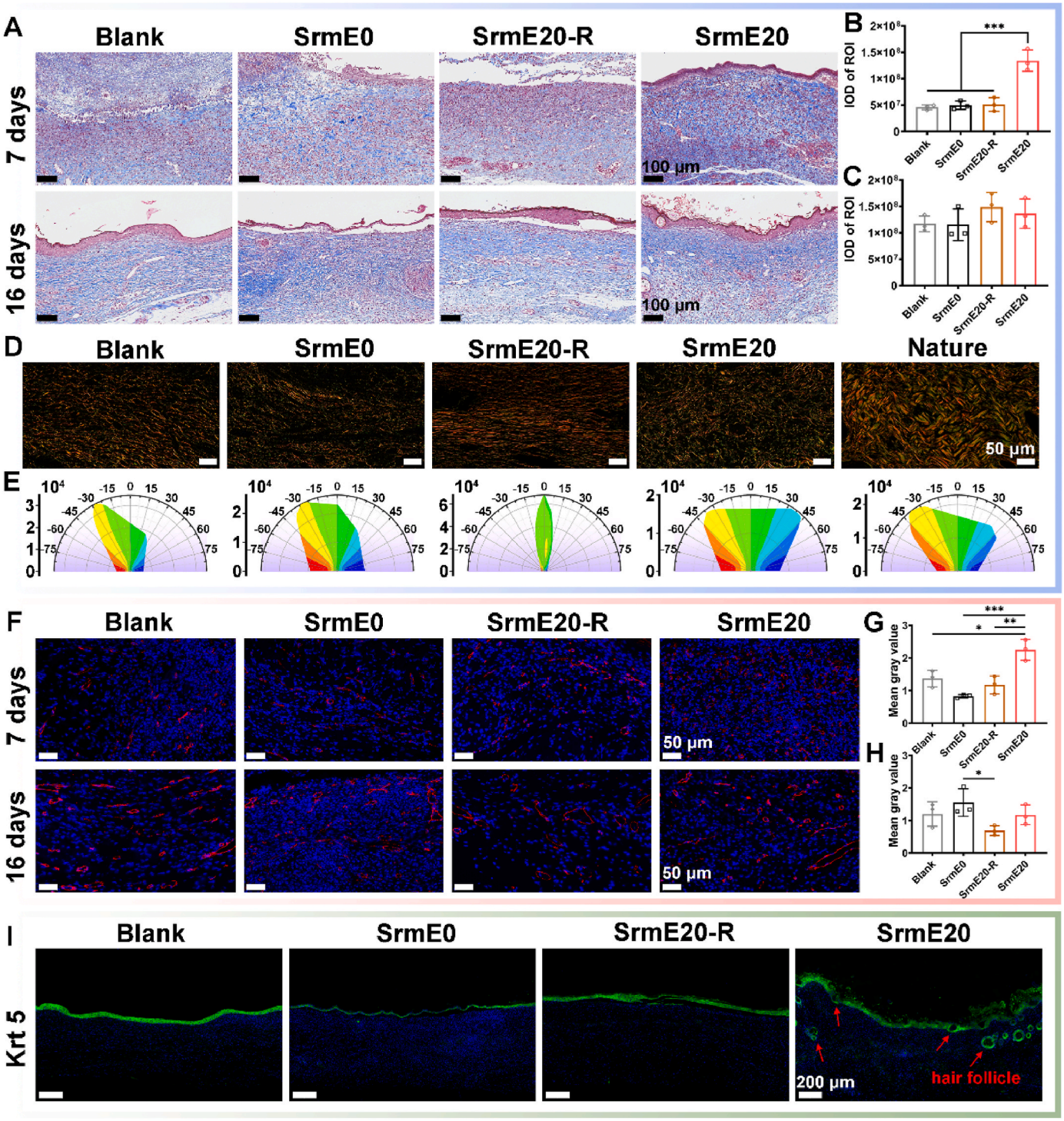

Fig. 7. (A) Masson staining and semi-quantitative statistics of collagen content at (B) seven days and (C) 16 days. (D) Sirius Red staining and (E) orientation distribution of collagen fibers at16 days. (F) CD31 immunostaining and semi-quantitative statistics at (G) seven days and (H) 16 days. (I) Krt 5 immunostaining of hair follicle at 16 days. *p < 0.05, **p < 0.01, and ***p < 0.001.

oxidized to quinones and lose their function, so it is important to balance the hydrogel's degree of crosslinking and phenolic hydroxyl's biochemical function. This study added EtOH to the hydrogel as a solvent to induce M1 polarization due to its widely reported ease of clearance and ability to induce inflammation in the liver [31–33]. The experiment confirmed an interesting phenomenon: Adding EtOH reduced the oxidation of phenolic hydroxyl groups by $NaIO_4$ and enhanced the mechanical properties of the hydrogel (Fig. 1B and C), possibly due to the antagonistic relationship between the EtOH-induced SF conformational changes and $NaIO_4$-triggered oxidative reaction. The hydrogel's free radical scavenging capacity and its β-sheet content increased with the EtOH concentration, proving that SF conformational changes and phenolic hydroxyl oxidation jointly participated in hydrogel crosslinking. More phenolic hydroxyl remained to play a role while ensuring the degree of crosslinking, providing a material foundation for inducing M2 macrophages.

Many hydrogel-type skin dressings, including a variety of effective ingredients and technologies, have been developed for the treatment of

infected wounds [18,27,28,37]. They eliminated bacteria through extra functional components, drugs, and antimicrobial peptides, but the wound healing depended on other mechanisms, which might not be consistent with the healing process of infected wounds.

In the face of mild infections that do not require additional assistance, the continuous polarization of macrophages is an important means by producing more M1 macrophages to clear bacteria, and then producing additional M2 cells for wound healing [45–47]. Compared to incorporate additional ingredients into skin dressings to achieve antibacterial and regenerative purposes, it is a good idea to use a material to time-sequentially drive the two phenotypic polarization of macrophages and intelligently enhance the effect of M1 and M2 macrophages. The innovative designed SrmE20 hydrogel could regulate the wound environment. Firstly, it exchanged ethanol with the environment to stimulate the polarization of M1 macrophages for enhancing the anti-bacterial effect. And then, the material effects of polyphenols and chitosan on macrophage differentiation were achieved after ethanol elimination to promote a M2 macrophage transformation. This intelligent regulatory process adapted to the regenerative microenvironment of infected wounds.

In the wounds of *S. aureus*-infected mice, SrmE20 cleared the bacteria colonized on the surface as scheduled, significantly reducing bacterial film production (Fig. 5). In addition, the activation of macrophages could enable the phagocytosis of bacteria infiltrating tissues (Fig. 6A) [36,37]. Due to the clearance of bacteria on the surface and inside of the wound, SrmE20 showed an apparent anti-inflammatory effect at three days, promoting macrophages' M2 polarization and entry into the wound healing phase. While CS and phenolic hydroxyl in the control groups reduced the number of bacteria, they could not enhance the effect of M1 macrophages to remove bacterial remnants, resulting in a significant inflammatory response persisting for a long time (Fig. 6B–F). Next, the sterile regeneration environment and accumulation of M2 macrophages in the later stage also stimulated earlier collagen deposition and angiogenesis, induced new skin tissue closer to normal skin in fiber arrangement, and generated new hair follicles at the wound edge. Therefore, this injectable immunoregulatory hydrogel promoted effective wound regeneration by sequentially driving phenotypic polarization of macrophage.

5. Conclusions

Here, an injectable immunoregulatory hydrogel was successfully constructed from CS-G and SF-D rich in phenolic hydroxyl groups/cations, using an EtOH/$NaIO_4$ solution as a composite crosslinker. The phenotype transformation of macrophages from M0 to M1 was achieved through the non-destructive encapsulation and release of EtOH, significantly inhibiting the adhesion and proliferation of bacteria *in vitro*. The phenolic hydroxyl groups and cations in the hydrogel's structure regulate the anti-inflammatory transformation of macrophages from M1 to M2, promoting the migration, adhesion, and proliferation of NIH-3T3 and BMSCs *in vitro*. The anti-contraction mouse infected skin wound model ($\Phi = 6$ mm) confirmed that this injectable immunoregulatory hydrogel effectively removed colonized bacteria on the surface and inside of the wound, accelerated the induction of M2 macrophage polarization, and promoted the generation of blood vessels and the restoration of matrix structure in the skin. This injectable immunoregulatory hydrogel, which can sequentially drive phenotypic polarization of macrophages, provided material design inspiration for the treatment of infected wounds.

Ethics approval and consent to participate

All animal studies were approved by the Sichuan University Medical Ethics Committee (KS2020330). All animal procedures were performed in accordance with the Guidelines for Care and Use of Laboratory Animals of Sichuan University.

CRediT authorship contribution statement

Yuxiang Wang: Writing – original draft, Visualization, Validation, Methodology, Investigation, Data curation, Conceptualization. **Chen Zhou:** Visualization, Methodology, Investigation. **Zhulian Li:** Visualization, Methodology, Investigation. **Gong Li:** Methodology, Investigation. **Yaping Zou:** Visualization, Methodology. **Xing Li:** Methodology, Conceptualization. **Peiyang Gu:** Visualization. **Jingyi Liu:** Methodology. **Lang Bai:** Validation, Resources. **Hong Yan:** Resources, Methodology. **Jie Liang:** Validation, Supervision, Software. **Xingdong Zhang:** Resources. **Yujiang Fan:** Writing – review & editing, Resources, Project administration, Funding acquisition, Conceptualization. **Yong Sun:** Writing – review & editing, Resources, Project administration, Funding acquisition, Conceptualization.

Declaration of competing interest

The authors declare that they have no known competing financial interests or personal relationships that could have appeared to influence the work reported in this paper.

Acknowledgements

The authors would like to thank Guolong Meng, Lingzhu Yu, and Jiao Lu of National Engineering Research Center for Biomaterials of Sichuan University for their technical support. This work was supported by the National Key R&D Project of China (No. 2022YFC2401800) and the National Natural Science Foundation of China (32071352 and 32271419).

Appendix A. Supplementary data

Supplementary data to this article can be found online at https://doi.org/10.1016/j.bioactmat.2024.07.015.

References

[1] N. Strbo, N. Yin, O. Stojadinovic, Innate and adaptive immune responses in wound epithelialization, Adv. Wound Care 3 (7) (2014) 492–501, https://doi.org/10.1089/wound.2012.0435.
[2] M. Malone, G. Schultz, Challenges in the diagnosis and management of wound infection, Br. J. Dermatol. 187 (2) (2022) 159–166, https://doi.org/10.1111/bjd.21612.
[3] R.A. Fisher, B. Gollan, S. Helaine, Persistent bacterial infections and persister cells, Nat. Rev. Microbiol. 15 (8) (2017) 453–464, https://doi.org/10.1038/nrmicro.2017.42.
[4] S. Lee, S. Inzerillo, G.Y. Lee, E.M. Bosire, S.K. Mahato, J. Song, Glycan-mediated molecular interactions in bacterial pathogenesis, Trends Microbiol. 30 (3) (2022) 254–267, https://doi.org/10.1016/j.tim.2021.06.011.
[5] T. Bjarnsholt, M. Whiteley, K.P. Rumbaugh, P.S. Stewart, P.Ø. Jensen, N. Frimodt-Møller, The importance of understanding the infectious microenvironment, Lancet Infect. Dis. 22 (3) (2022) e88–e92, https://doi.org/10.1016/S1473-3099(21)00122-5.
[6] J.P. Burnham, J.P. Kirby, M.H. Kollef, Diagnosis and management of skin and soft tissue infections in the intensive care unit: a review, Intensive Care Med. 42 (2016) 1899–1911, https://doi.org/10.1007/s00134-016-4576-0.
[7] D. Limmathurotsakul, S. Dunachie, K. Fukuda, N.A. Feasey, I.N. Okeke, A. H. Holmes, C.E. Moore, C. Dolecek, H.R. van Doorn, N. Shetty, A.D. Lopez, S. J. Peacock, Improving the estimation of the global burden of antimicrobial resistant infections, Lancet Infect. Dis. 19 (11) (2019) e392–e398, https://doi.org/10.1016/S1473-3099(19)30276-2.
[8] Y. Wang, Y.N. Yang, Y.R. Shi, H. Song, C.Z. Yu, Antibiotic-free antibacterial strategies enabled by nanomaterials: progress and perspectives, Adv. Mater. 32 (18) (2019) 1904106, https://doi.org/10.1002/adma.201904106.
[9] C.H. Chen, L. Chen, C.Y. Mao, L.G. Jin, S.L. Wu, Y.F. Zheng, Z.D. Cui, Z.Y. Li, Y. Zhang, S.L. Zhu, H. Jiang, X.M. Liu, Natural extracts for antibacterial applications, Small 20 (9) (2023) 2306553, https://doi.org/10.1002/smll.202306553.
[10] S.Y. Cheng, H. Wang, X.H. Pan, C. Zhang, K.X. Zhang, Z.L. Chen, W. Dong, A. M. Xie, X.L. Qi, Dendritic hydrogels with robust inherent antibacterial properties for promoting bacteria-infected wound healing, ACS Appl. Mater. Interfaces 14 (9) (2022) 11144–11155, https://doi.org/10.1021/acsami.1c25014.
[11] C.F. Zhang, E.Y. Cai, X.L. Qi, X.X. Ge, Y.J. Xiang, J.J. Wang, Y. Li, L.Z. Lv, H. Zheng, Y.N. Qian, W. Dong, H. Li, J.L. Shen, Immunomodulatory gallium/glycyrrhizic acid hydrogels for treating multidrug-resistant *Pseudomonas aeruginosa*-infected

pressure ulcers, Chem. Eng. J. 487 (2024) 150756, https://doi.org/10.1016/j.cej.2024.150756.
[12] X.L. Qi, X.X. Ge, X.J. Chen, E.Y. Cai, Y.J. Xiang, H.B. Hu, Y. Li, Y.L. Lan, Y.Z. Shi, H. Deng, J.L. Shen, An immunoregulation hydrogel with controlled hyperthermia-augmented oxygenation and ROS scavenging for treating diabetic foot ulcers, Adv. Funct. Mater. (2024) 2400489, https://doi.org/10.1002/adfm.202400489.
[13] M. Kharaziha, A. Baidya, N. Annabi, Rational design of immunomodulatory hydrogels for chronic wound healing, Adv. Mater. 33 (39) (2021) 2100176, https://doi.org/10.1002/adma.202100176.
[14] M.M. Alvarez, J.C. Liu, G. Trujillo-de Santiago, B.H. Cha, A. Vishwakarma, A. M. Ghaemmaghami, A. Khademhosseini, Delivery strategies to control inflammatory response: modulating M1–M2 polarization in tissue engineering applications, J. Contr. Release 240 (2016) 349–363, https://doi.org/10.1016/j.jconrel.2016.01.026.
[15] Y.P. Zou, C. Zhou, Z.L. Li, X.W. Han, L. Tong, T.J.H. Liu, L. Xiong, L. Bai, J. Liang, Y.J. Fan, X.D. Zhang, Y. Sun, Hydrophobic tetracycline immobilized in fibrous hyaluronan regulates adhesive collagen-based hydrogel stability for infected wound healing, Small 19 (45) (2023) 2303414, https://doi.org/10.1002/smll.202303414.
[16] H.X. Huang, Y.Y. Xie, J. Zhong, Z.Y. Fu, P.U. Wu, X.Q. Chen, Z.Q. Xiao, J. Yuan, X. T. Shi, D. Liang, Antimicrobial peptides loaded collagen nanosheets with enhanced antibacterial activity, corneal wound healing and M1 macrophage polarization in bacterial keratitis, Composites, Part B 275 (2024) 111283, https://doi.org/10.1016/j.compositesb.2024.111283.
[17] Q.Q. Feng, X.T. Ma, K.M. Cheng, G.N. Liu, Y. Li, Y.L. Yue, J. Liang, L.Z. Zhang, T. J. Zhang, X.W. Wang, X.Y. Gao, G.J. Nie, X. Zhao, Engineered bacterial outer membrane vesicles as controllable two-way adaptors to activate macrophage phagocytosis for improved tumor immunotherapy, Adv. Mater. 34 (40) (2022) 2206200, https://doi.org/10.1002/adma.202206200.
[18] Z.L. Tu, M. Chen, M. Wang, Z.X. Shao, X.Q. Jiang, K.Y. Wang, Z. Yao, S.W. Yang, X. X. Zhang, W.Y. Gao, C. Lin, B. Lei, C. Mao, Engineering bioactive M2 macrophage-polarized anti-inflammatory, antioxidant, and antibacterial scaffolds for rapid angiogenesis and diabetic wound repair, Adv. Funct. Mater. 31 (30) (2021) 2100924, https://doi.org/10.1002/adfm.202100924.
[19] J.Y. Mao, L. Chen, Z.W. Cai, S.T. Qian, Z.M. Liu, B.F. Zhao, Y.G. Zhang, X.M. Sun, W.G. Cui, Advanced biomaterials for regulating polarization of macrophages in wound healing, Adv. Funct. Mater. 32 (12) (2021) 2111003, https://doi.org/10.1002/adfm.202111003.
[20] P. Pantazi, T. Clements, M. Venø, V.M. Abrahams, B. Holder, Distinct non-coding RNA cargo of extracellular vesicles from M1 and M2 human primary macrophages, J. Extracell. Vesicles 11 (12) (2022) 12293, https://doi.org/10.1002/jev2.12293.
[21] L.B. Pang, P.F. Tian, X. Cui, X.P. Wu, X.L. Zhao, H. Wang, D.P. Wang, H.B. Pan, In situ photo-cross-linking hydrogel accelerates diabetic wound healing through restored hypoxia-inducible factor 1-alpha pathway and regulated inflammation, ACS Appl. Mater. Interfaces 13 (25) (2021) 29363–29379, https://doi.org/10.1021/acsami.1c07103.
[22] P. Wang, B.R. Wu, M. Li, Y.C. Song, C.J. Chen, G.X. Feng, D. Mao, F. Hu, B. Liu, Lysosome-targeting aggregation-induced emission nanoparticle enables adoptive macrophage transfer-based precise therapy of bacterial infections, ACS Nano 17 (11) (2023) 10365–10375, https://doi.org/10.1021/acsnano.3c00796.
[23] K. Xie, N.Q. Wang, Y. Guo, S. Zhao, J. Tan, L. Wang, G.Y. Li, J.X. Wu, Y.Z. Yang, W. Y. Xu, J. Chen, W.B. Jiang, P.H. Fu, Y.Q. Hao, Additively manufactured biodegradable porous magnesium implants for elimination of implant-related infections: an in vitro and in vivo study, Bioact. Mater. 8 (2022) 140–152, https://doi.org/10.1016/j.bioactmat.2021.06.032.
[24] F. Wang, Q.H. Wu, C.F. Zhang, L.C. Kong, R.T. Zuo, K. Feng, G.P. Jia, M.F. Hou, J. H. Zou, Y.M. Chai, J. Xu, X.Y. Chen, Q.L. Kang, Ultrasmall MnOx nanodots catalyze glucose for reactive oxygen species-dependent sequential anti-infection and regeneration therapy, Small Struct. 5 (1) (2023) 2300198, https://doi.org/10.1002/sstr.202300198.
[25] X.M. Li, R.E. Xing, C.J. Xu, S. Liu, Y.K. Qin, K.C. Li, H.H. Yu, P.C. Li, Immunostimulatory effect of chitosan and quaternary chitosan: a review of potential vaccine adjuvants, Carbohydr. Polym. 264 (2021) 118050, https://doi.org/10.1016/j.carbpol.2021.118050.
[26] X.Y. Wang, Y.L. Fan, J.J. Yan, M. Yang, Engineering polyphenol-based polymeric nanoparticles for drug delivery and bioimaging, Chem. Eng. J. 439 (2022) 135661, https://doi.org/10.1016/j.cej.2022.135661.
[27] Y. Duan, F.C. Jiang, Q. Li, A. McDowell, Y.X. Li, Y. Wang, S. Liu, C. Zhang, X.l. Pan, Multifunctional polysaccharide/metal/polyphenol double-crosslinked hydrogel for infected wound, Carbohydr. Polym. 332 (2024) 121912, https://doi.org/10.1016/j.carbpol.2024.121912.
[28] X.L. Wei, C.K. Liu, Z.Q. Li, Z.X. Gu, J.X. Yang, K. Luo, Chitosan-based hydrogel dressings for diabetic wound healing via promoting M2 macrophage-polarization, Carbohydr. Polym. 331 (2024) 121873, https://doi.org/10.1016/j.carbpol.2024.121873.
[29] N. Xu, Y.P. Gao, Z. Li, Y. Chen, M.L. Liu, J.Z. Jia, R. Zeng, G.X. Luo, J.F. Li, Y.L. Yu, Immunoregulatory hydrogel decorated with Tannic acid/Ferric ion accelerates diabetic wound healing via regulating macrophage polarization, Chem. Eng. J. 466 (2023) 143173, https://doi.org/10.1016/j.cej.2023.143173.
[30] Y.H.Z. Feng, H.L. Gao, D. Wu, Y.T. Weng, Z.Y. Wang, S.H. Yu, Z.L. Wang, Biomimetic lamellar chitosan scaffold for soft gingival tissue regeneration, Adv. Funct. Mater. 31 (43) (2021) 2105348, https://doi.org/10.1002/adfm.202105348.
[31] M. Wang, G.N. Shen, L.G. Xu, X.D. Liu, J.M. Brown, D.C. Feng, R.A. Ross, B. Gao, S. Liangpunsakul, C. Ju, IL-1 receptor like 1 protects against alcoholic liver injury by limiting NF-κB activation in hepatic macrophages, J. Hepatol. 68 (1) (2018) 109–117, https://doi.org/10.1016/j.jhep.2017.08.023.
[32] V. Marin, K. Poulsen, G. Odena, M.R. McMullen, J. Altamirano, P. Sancho-Bru, C. Tiribelli, J. Caballeria, N. Rosso, R. Bataller, L.E. Nagy, Hepatocyte-derived macrophage migration inhibitory factor mediates alcoholinduced liver injury in mice and patients, J. Hepatol. 67 (5) (2017) 1018–1025, https://doi.org/10.1016/j.jhep.2017.06.014.
[33] H. Zhou, M.J. Yu, J.J. Zhao, B.N. Martin, S. Roychowdhury, M.R. McMullen, E. Wang, P.L. Fox, S. Yamasaki, L.E. Nagy, X.X. Li, IRAKM-Mincle axis links cell death to inflammation: pathophysiological implications for chronic alcoholic liver disease, Hepatology 64 (6) (2016) 1978–1993, https://doi.org/10.1002/hep.28811.
[34] M. Gholipourmalekabadi, S. Sapru, A. Samadikuchaksaraei, R.L. Reis, D.L. Kaplan, S.C. Kundu, Silk fibroin for skin injury repair: where do things stand? Adv. Drug Deliv. Rev. 153 (2020) 28–53, https://doi.org/10.1016/j.addr.2019.09.003.
[35] C. Sohn, H. Kim, J. Han, K.-T. Lee, A. Šutka, C.K. Jeong, Generating electricity from molecular bonding-correlated piezoresponse of biodegradable silk nanofibers, Nano Energy 103 (2022) 107844, https://doi.org/10.1016/j.nanoen.2022.107844.
[36] C. Gao, C.H.T. Kwong, M. Tang, J.W. Liu, H. Kam, S.K. Li, S.M.Y. Lee, C.H. Fan, H. Z. Yu, R.B. Wang, A bacterially engineered macrophage sponge as a neutralization decoy to treat bacterial infection, Matter 6 (11) (2023) 3889–3911, https://doi.org/10.1016/j.matt.2023.09.007.
[37] Y. Meng, L.J. Chen, Y. Chen, J.Y. Shi, Z. Zhang, Y.W. Wang, F. Wu, X.W. Jiang, W. Yang, L. Zhang, C.C. Wang, X.F. Meng, Y.L. Wu, W.B. Bu, Reactive metal boride nanoparticles trap lipopolysaccharide and peptidoglycan for bacteria-infected wound healing, Nat. Commun. 13 (1) (2022) 7353, https://doi.org/10.1038/s41467-022-35050-6.
[38] Y.W. Zhang, S.F. Ai, Z.M. Yu, L.X. Wang, H. Tao, B. Wang, D.L. Kong, Z.M. Yang, Y. B. Wang, Mesenchymal stem cell spheroids induced by supramolecular nanofibers for diabetic wound healing, Adv. Funct. Mater. (2024) 2314607, https://doi.org/10.1002/adfm.202314607.
[39] L.H. Luo, S.J. Wang, Y.L. Hu, L.T. Wang, X.D. Jiang, J.L. Zhang, X. Liu, X.M. Guo, Z. Y. Luo, C.Q. Zhu, M.M. Xie, Y.Q. Li, J. You, F.C. Yang, Precisely regulating M2 subtype macrophages for renal fibrosis resolution, ACS Nano 17 (22) (2023) 22508–22526, https://doi.org/10.1021/acsnano.3c05998.
[40] C. Maier, A. Ramming, C. Bergmann, R. Weinkam, N. Kittan, G. Schett, J.H. W. Distler, C. Beyer, Inhibition of phosphodiesterase 4 (PDE4) reduces dermal fibrosis by interfering with the release of interleukin-6 from M2 macrophages, Ann. Rheum. Dis. 76 (6) (2017) 1133–1141, https://doi.org/10.1136/annrheumdis-2016-210189.
[41] L. Kaps, A. Huppertsberg, N. Choteschovsky, A. Klefenz, F. Durak, B. Schrörs, M. Diken, E. Eichler, S. Rosigkeit, S. Schmitt, C. Leps, A. Schulze, F. Foerster, E. Bockamp, B.G. De Geest, K. Koynov, H.J. Räder, S. Tenzer, F. Marini, D. Schuppan, L. Nuhn, pH-degradable, bisphosphonate-loaded nanogels attenuate liver fibrosis by repolarization of M2-type macrophages, Proc. Natl. Acad. Sci. U.S. A. 119 (12) (2022) e2122310119, https://doi.org/10.1073/pnas.2122310119.
[42] Y.Q. Yan, W. Jiang, L. Liu, X.Q. Wang, C. Ding, Z.G. Tian, R.B. Zhou, Dopamine controls systemic inflammation through inhibition of nlrp3 inflammasome, Cell 160 (1–2) (2015) 62–73, https://doi.org/10.1016/j.cell.2014.11.047.
[43] X. Li, Z.L. Li, P.L. Wang, G.G. Lu, L. Tong, Q.Y. Liu, Y.F. Chen, J.L. Lin, E. Luo, J. Liang, Q. Jiang, Y.J. Fan, X.D. Zhang, Y. Sun, Dopamine-integrated nanointerface between fibrillar matrix and hydrophilic nanohydroxyapatite regulates immune microenvironment to boost endogenous bone regeneration, Adv. Funct. Mater. 33 (16) (2023) 2212738, https://doi.org/10.1002/adfm.202212738.
[44] N.B. Bone, Z.Y. Liu, J.-F. Pittet, J.W. Zmijewski, Frontline Science: D1 dopaminergic receptor signaling activates the AMPK-bioenergetic pathway in macrophages and alveolar epithelial cells and reduces endotoxin-induced ALI, J. Leukoc. Biol. 101 (2) (2017) 357–365, https://doi.org/10.1189/jlb.3HI0216-068RR.
[45] M. Sharifiaghdam, E. Shaabani, R. Faridi-Majidi, S.C. De Smedt, K. Braeckmans, J. C. Fraire, Macrophages as a therapeutic target to promote diabetic wound healing, Mol. Ther. 30 (9) (2022) 2891–2908, https://doi.org/10.1016/j.ymthe.2022.07.016.
[46] D. Gay, G. Ghinatti, C.F. Guerrero-Juarez, R.A. Ferrer, F. Ferri, C.H. Lim, S. Murakami, N. Gault, V. Barroca, I. Rombeau, P. Mauffrey, L. Irbah, E. Treffeisen, S. Franz, A. Boissonnas, C. Combadière, M. Ito, M.V. Plikus, P.H. Romeo, Phagocytosis of Wnt inhibitor SFRP4 by late wound macrophages drives chronic Wnt activity for fibrotic skin healing, Sci. Adv. 6 (12) (2020) eaay3704, https://doi.org/10.1126/sciadv.aay3704.
[47] A. Joorabloo, T.Q. Liu, Recent advances in nanomedicines for regulation of macrophages in wound healing, J. Nanobiotechnol. 20 (1) (2022) 407, https://doi.org/10.1186/s12951-022-01616-1.